GEOLOGY | THE GEOLOGICAL SOCIETY OF AMERICA®

https://doi.org/10.1130/G49732.1

Manuscript received 29 September 2021
Revised manuscript received 3 March 2022
Manuscript accepted 8 March 2022

Published online 9 May 2022

Cenozoic delamination of the southwestern Yangtze craton owing to densification during subduction and collision

Jun Wang[1,2], Qiang Wang[1,2,3]*, Chuan-Bing Xu[1,2,3], Wei Dan[1,2]*, Zhuo Xiao[1,2], Chutian Shu[4] and Gangjian Wei[1,2]

[1]State Key Laboratory of Isotope Geochemistry, Guangzhou Institute of Geochemistry, Chinese Academy of Sciences, Guangzhou 510640, China

[2]CAS Center for Excellence in Deep Earth Science, Guangzhou 510640, China

[3]College of Earth and Planetary Sciences, University of Chinese Academy of Sciences, Beijing 100049, China

[4]School of Natural Sciences, Macquarie University, Sydney, New South Wales 2109, Australia

ABSTRACT

It is widely thought that oceanic subduction can trigger cratonic keel delamination, but the southwestern Yangtze craton (SYC; southwestern China) lost its lower keel during Cenozoic continental collision. The upper mantle beneath the thinned SYC contains its incompletely delaminated keel, which has high-velocity seismic anomalies. Combining geophysical observations with the geochemistry of Eocene mafic potassic lavas derived from the SYC mantle at different depths, we suggest that the deep (~130 km) delaminated lithosphere was more fertile and dense, with low-forsterite (Fo; molar 100 × Mg/[Mg + Fe] = 91.3) and high-$\delta^{18}O$ (5.9‰) olivine, than the shallow (~55 km) intact lithosphere (Fo = 94.2; $\delta^{18}O$ = 5.2‰), although both were rehydrated and oxidized. The deep keel underwent strong refertilization and densification owing to the addition of Fe-rich basaltic melts during earlier oceanic subduction. Subduction-driven refertilization and subsequent collision-driven cooling caused cratonic keel delamination due to compositional and thermal densification rather than hydration- or oxidation-induced rheological weakening. Our study provides an example of Cenozoic cratonic keel delamination in a collisional orogen and highlights the key roles of compositional and thermal densification in delamination during subduction and collision.

INTRODUCTION

Cratons with thick (as much as 250 km) mantle keels have been isolated from mantle convection for more than 2 b.y. due to their melt-depleted and refractory nature. However, some cratons lost their keels during oceanic subduction (Lee et al., 2011; Wu et al., 2019) because subduction-related melts may change the mantle viscosity by rehydration (Hirth and Kohlstedt, 1996) and oxidation (Cline et al., 2018) and change mantle density by refertilization (Lee et al., 2011). However, recent experiments suggest a limited effect of H_2O on mantle rheology (Fei et al., 2013). Thus, our understanding of the relative contribution to cratonic instability from different factors (e.g., H_2O, oxygen fugacity [f_{O2}], and density) remains poor and conflicting. This may be due to our lack of knowledge of the nature of cratonic keels that have sunk into the deep mantle.

The thickness of the southwestern Yangtze craton (SYC; southwestern China) shows a decrease from its interior (as thick as 200 km beneath the Sichuan Basin) to its southwestern margin (<80 km thick; Fig. 1; An and Shi, 2006; Yang et al., 2017), indicating that part of the SYC keel has been removed. The deeper upper mantle contains high-seismic-velocity bodies that are connected to the interior cratonic mantle, implying the keel is incompletely delaminated (Fig. 1C; Huang et al., 2019; Lei et al., 2019). This delamination during the India-Asia collision generated potassic magmatism at 37–33 Ma by melting of the lithospheric mantle (Fig. 1B; Lu et al., 2015). This magmatism can constrain the nature of the SYC lithospheric mantle at different depths, which might shed light on the causes of cratonic keel delamination in collisional orogens.

SAMPLES AND RESULTS

The SYC is separated from the Indochina block to the southwest by the Ailaoshan–Red River fault (Fig. 1B). Northward subduction of the Paleotethys Ocean beneath the integrated SYC and Indochina block during the Paleozoic produced the Ailaoshan back-arc oceanic basin. Bipolar subduction of the Ailaoshan Ocean during the Permian–Triassic caused further mantle metasomatism of the SYC margin (Wang et al., 2018). There is no post-Triassic magmatism in the SYC apart from abundant potassic rocks formed after the India-Asia collision. We collected Eocene mafic potassic lavas from the Dali and Yanyuan areas (Fig. 1B), which were erupted on thin (~70 km) and thick (~120 km) lithosphere, respectively. All the samples are porphyritic, with olivine, clinopyroxene, and phlogopite phenocrysts, but the Dali lavas have larger phenocrysts than the Yanyuan lavas (Fig. S1 in the Supplemental Material[1]). Some Dali samples contain diabasic lithic fragments that consist mainly of feldspar and clinopyroxene. These fragments are not aggregates of phenocrysts, given that their host rocks lack feldspar phenocrysts (Fig. S1). Olivine phenocrysts contain spinel and melt inclusions (Fig. S2). The analytical and data processing methods are described in the Supplemental Material.

The Dali lavas are basaltic trachyandesites with higher SiO_2 contents (51.8–56.2 wt%; on an anhydrous basis) but lower CaO, FeO_T (total Fe), Sm/Yb, and La/Yb than the Yanyuan trachybasalts (SiO_2 = 46.4–48.2 wt%) (Fig. 2). The Dali olivines have lower CaO contents (<0.1 wt%) than the Yanyuan olivines at the same forsterite values (Fo; molar 100 × Mg/[Mg + Fe]), but the maximum olivine Fo (94.2)

*E-mails: wqiang@gig.ac.cn; danwei@gig.ac.cn

[1]Supplemental Material. Methods, Tables S1–S9, and Figures S1–S6. Please visit https://doi.org/10.1130/GEOL.S.19593451 to access the supplemental material, and contact editing@geosociety.org with any questions.

CITATION: Wang, J., et al., 2022, Cenozoic delamination of the southwestern Yangtze craton owing to densification during subduction and collision: Geology, v. 50, p. 912–917, https://doi.org/10.1130/G49732.1

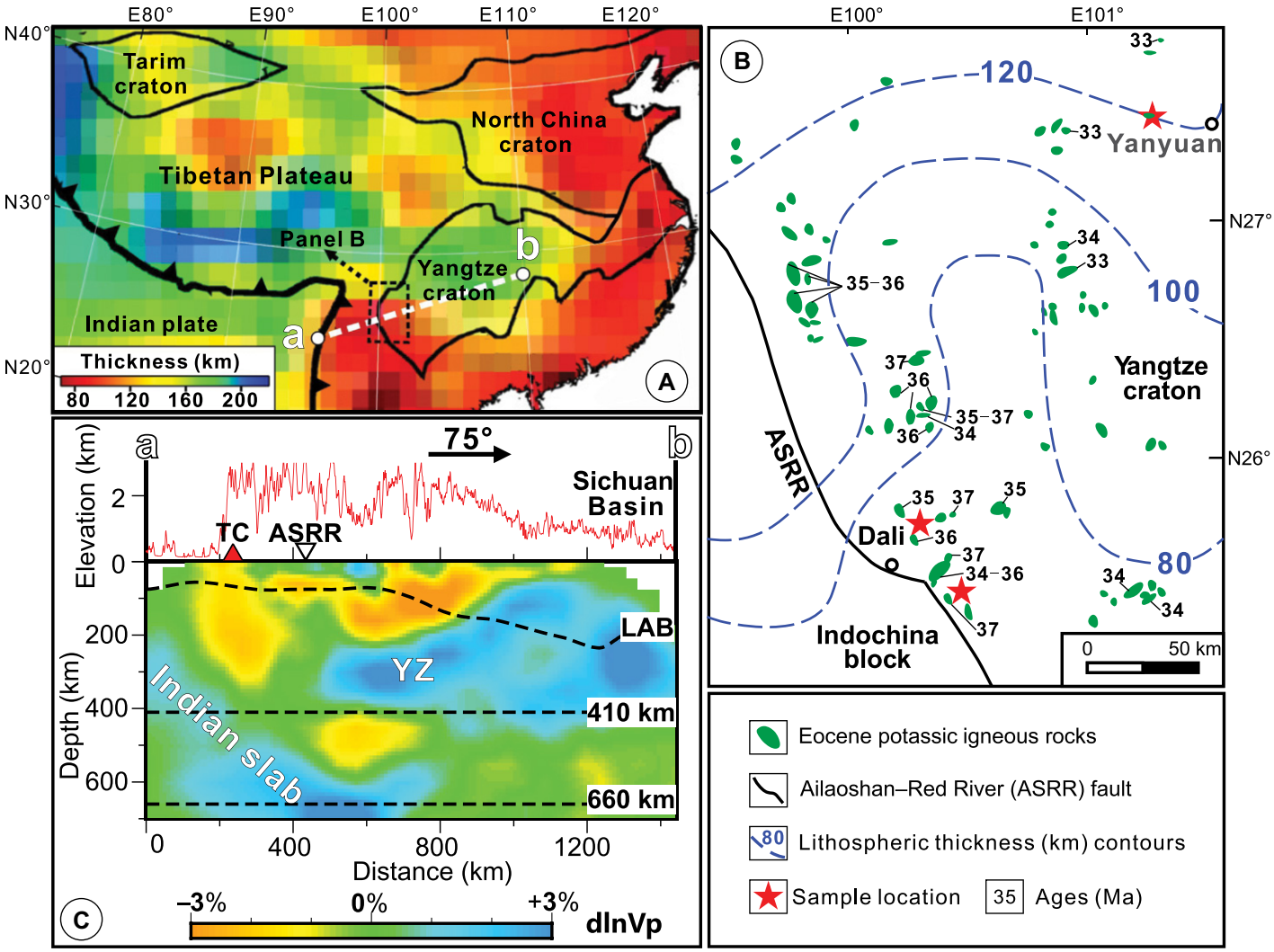

Figure 1. (A) Seismic-thermal lithospheric thickness in China (An and Shi, 2006). (B) Geological map showing Eocene magmatism (Lu et al., 2015), lithospheric thickness contours (Yang et al., 2017), and sample locations in the southwestern Yangtze craton. (C) Topography and P-wave tomography along profile a–b in panel A and lithosphere-asthenosphere boundary (LAB) based on other models (Huang et al., 2019). YZ—delaminated Yangtze keel; TC—Tengchong volcano.

and NiO (0.64 wt%) contents and spinel Cr# values (molar Cr/[Cr + Al] = 0.84–0.90) of the Dali lavas are higher than those of the Yanyuan lavas (Fo = 91.3; NiO = 0.56 wt%; Cr# = 0.71–0.73; Figs. 3A–3C). The olivine-spinel oxybarometer of Ballhaus et al. (1991) is valid under oxidized conditions and yields f_{O_2} values of FMQ (fayalite-magnetite-quartz) + 1.9 (±0.3; 1σ; n = 59) for the Dali lavas and FMQ + 1.5 (±0.1; 1σ; n = 20) for the Yanyuan lavas. The difference between the two results and uncertainty contributed by the spinel analysis are within the precision (±0.4 log units) of the oxybarometer (Fig. 3C). The horizontal trend between f_{O_2} and Fo values indicates f_{O_2} was constant during magmatic differentiation (Fig. 3C). Many Dali olivine phenocrysts exhibit decreasing Fo and increasing $\delta^{18}O$ values toward crystal rims (Fig. S2), forming negative correlations between Fo, NiO, and $\delta^{18}O$ (Figs. 3E and 3F). In contrast, the Yanyuan olivine phenocrysts are relatively homogeneous and show a horizontal trend between $\delta^{18}O$ and NiO (Fig. 3F; Fig. S2).

DISCUSSION

Magmatic Phenocrysts or Mantle Xenocrysts?

The high-Fo (>89) olivine phenocrysts in the Dali lavas have CaO < 0.1 wt%, similar to mantle xenocrysts. However, the following evidence suggests a magmatic origin:

(1) High-Fo olivines occur as the cores of euhedral phenocrysts and lack the deformation (e.g., kink bands) and dissolution textures (Fig. S2R) that characterize mantle xenocrysts.

(2) Some olivine cores contain oval melt inclusions that are isolated without healed cracks (Fig. S2)

(3) Spinel inclusions in olivine (Fig. S2) are euhedral, but mantle spinel is anhedral or vermicular and distributed along grain boundaries (Kamenetsky et al., 2006).

(4) The high-Fo (>92) olivines are in Fe-Mg equilibrium with their host rock (Fig. S4), indicating crystallization from the host rock.

(5) The Dali olivines have lower CaO and P_2O_5 contents than the Yanyuan olivines at a given Fo value, similar to their corresponding host rocks (Figs. 2B and 3A; Fig. S3). Thus, the low-Ca feature of olivine was inherited from the parental magmas.

Water can also inhibit the partitioning of Ca into olivine, as evident from the extreme Ca depletions of some arc olivines (Fig. 3A; Kamenetsky et al., 2006). Magmatic H_2O contents can be estimated from the partition coefficient for CaO between olivine and host rocks (Gavrilenko et al., 2016). Using the high-Fo olivines in Fe-Mg equilibrium with their host rocks (Fig. S4), we obtained H_2O contents of 6.7 ± 0.9 wt% (1σ; n = 43) and 6.0 ± 0.2 wt% (1σ; n = 34) for the Dali and Yanyuan lavas, respectively (Fig. 3D).

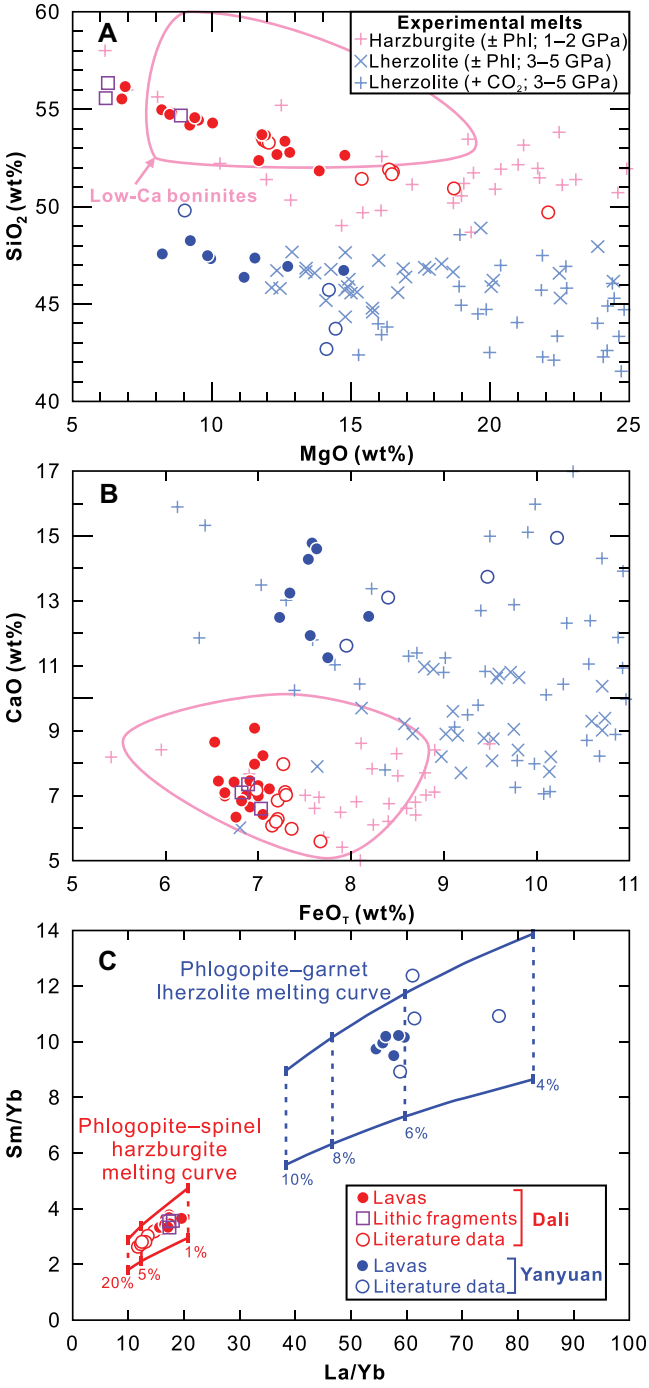

Figure 2. Major and trace element data for the southwestern Yangtze craton (China) potassic lavas. The two curves for each lava type represent two enriched spinel- and garnet-facies mantle sources with different REE compositions. Data sources for samples analyzed in previous studies, experimental peridotite melts (±phlogopite [Phl] or CO_2), low-Ca boninites, and melt modeling parameters are provided in the Supplemental Material (see footnote 1).

Mantle Source Characteristics

The potassic ($K_2O/Na_2O > 1$) feature of mantle-derived magmas is attributed to phlogopite breakdown during peridotite or pyroxenite melting (Ammannati et al., 2016; Condamine et al., 2016). An example of potassic rocks generated by melting of phlogopite pyroxenite is lamproites in Italy (Ammannati et al., 2016). The studied olivines have lower NiO contents at a given Fo value (Fig. 3B) than those in Italian lamproites but overlap with those crystallized from peridotite-derived melts, indicating a source dominated by phlogopite peridotite. Olivine-spinel pairs in the Dali lavas are similar to those in low-Ca boninites in terms of olivine Fo and CaO contents and spinel Cr# values (Figs. 3A–3C), and their host rocks also have similar SiO_2, MgO, CaO, and FeO contents (Figs. 2A and 2B). These similarities indicate the involvement of shallow, hydrous, and ultradepleted harzburgite in their mantle source (Prelević and Foley, 2007). Experimental melts of harzburgite (±phlogopite) generated at 1–2 GPa also overlap the composition of the Dali lavas (Figs. 2A and 2B). In contrast, the Yanyuan lavas with high CaO contents are similar to melts of carbonated lherzolites generated at 3–5 GPa (Fig. 2B). Their high Nb/Ta ratios (29 ± 1) and the occurrence of carbonatites (34–11 Ma) north of Yanyuan also indicate the presence of carbonated mantle (Hou et al., 2015). Carbonate metasomatism would yield an olivine-rich mantle (Ammannati et al., 2016). Rare earth element (REE) modeling shows that the Dali and Yanyuan lavas could have been produced by non-modal batch melting of light-REE–enriched phlogopite-bearing spinel harzburgite and garnet lherzolite, respectively (Fig. 2C). Mantle-melt barometry for the high-MgO (>9 wt%) samples indicates that the Dali and Yanyuan primary melts formed at 1.7 ± 0.1 GPa (1σ; $n = 12$) and 4.0 ± 0.1 GPa (1σ; $n = 7$), respectively (Table S1). A shallower origin for the Dali lavas is consistent with low-pressure andesitic melts derived by the preferential melting of Si-rich orthopyroxene in phlogopite harzburgite (Fig. 2A; Condamine et al., 2016).

The maximum olivine Fo and NiO contents and spinel Cr# values of the Yanyuan lavas are lower than for the Dali lavas (Figs. 3B and 3C). The difference in olivine Fo values cannot be explained by the magmatic f_{O2} because both types of lavas were oxidized with similar f_{O2} (Fig. 3C). Fo values of olivine crystallizing in a primary magma should be similar to those in its mantle source. Thus, the mantle source of the Yanyuan lavas was more fertile, with lower Cr/Al ratios, lower-Fo (91.3) olivine, and more Ca-rich pyroxene than that (Fo = 94.2) of the Dali lavas.

High-Fo (>93) olivines with $\delta^{18}O = 5.2‰ \pm 0.1‰$ in the Dali lavas suggest their primary magmas originated from normal $\delta^{18}O$ mantle (Mattey et al., 1994; Fig. 3E). Negative correlations between olivine $\delta^{18}O$ values and Fo and NiO contents imply the high $\delta^{18}O$ values resulted from combined assimilation and fractional crystallization because olivine fractionation alone cannot produce a large increase in $\delta^{18}O$ (Figs. 3E and 3F). The likely assimilant was the diabasic lithic fragments with a dissolution boundary (Fig. S1). These fragments are cognate with the host lavas because they have similar whole-rock (Fig. 2) and clinopyroxene (Fig. S5) compositions and thus represent earlier dikes that may have had high $\delta^{18}O$ due to low-temperature hydrothermal alteration. Such self-cannibalization of cognate mafic rocks has little effect on the elements and radiogenic isotopes of basalts (Bindeman, 2008). In contrast, the horizontal trend between $\delta^{18}O$ and NiO values for the Yanyuan olivines indicates crystallization from magma in equilibrium with high-$\delta^{18}O$ (5.9‰ ± 0.1‰) mantle olivine (Fig. 3F).

Therefore, the deep (131 ± 5 km) lithospheric mantle was more fertile than the shallow (55 ± 3 km) lithospheric mantle. The former likely consisted of refertilized lherzolites formed by mantle metasomatism, rather than less-depleted peridotite produced during craton

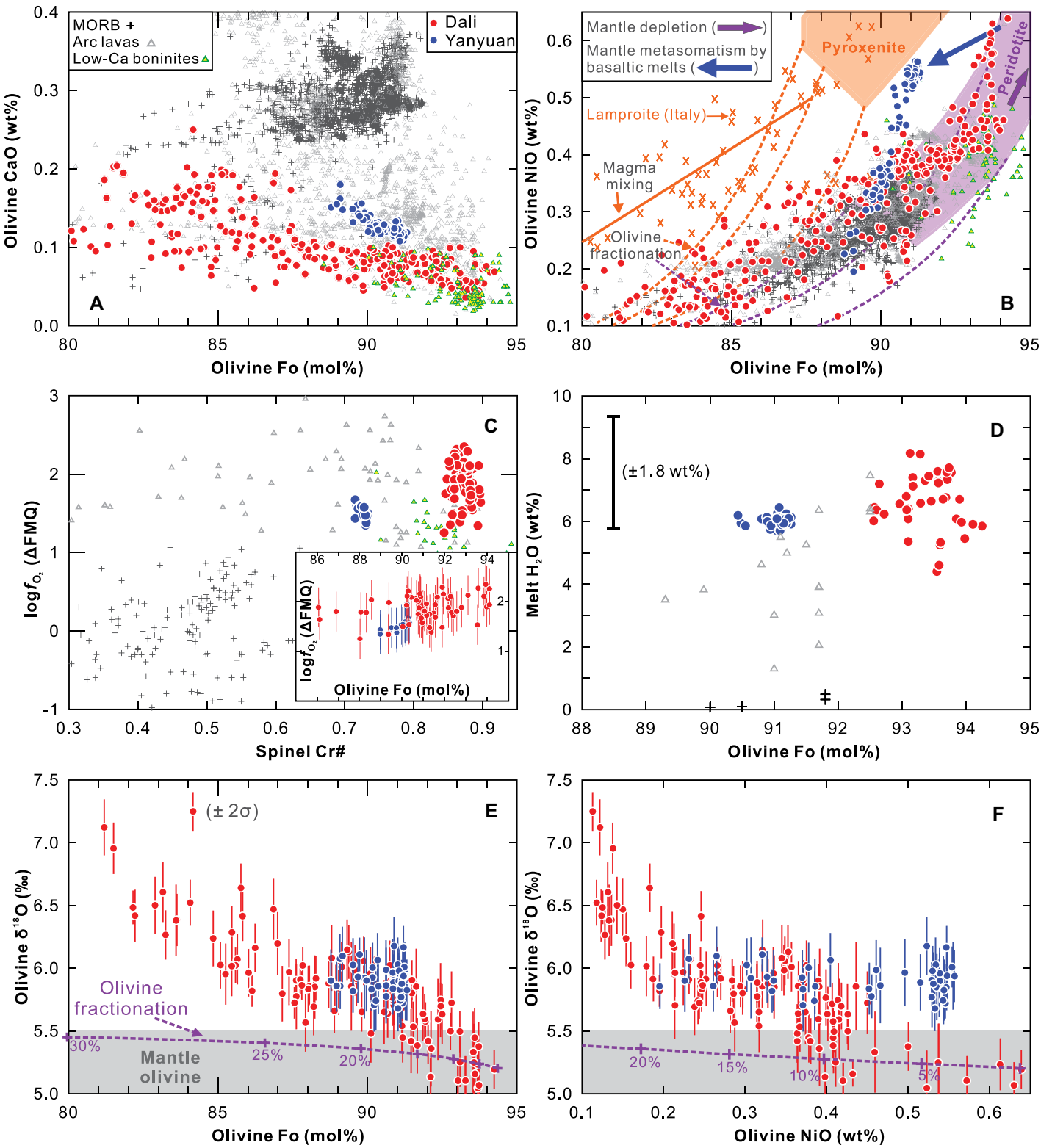

Figure 3. (A–D) Comparison of olivines and spinel inclusions from the southwestern Yangtze craton (China) potassic lavas with those in mid-oceanic ridge basalts (MORB), Italian lamproites, arc lavas, and low-Ca boninites. Olivine fractionation and magma mixing lines and peridotite and pyroxenite melting fields are from Straub et al. (2008). Forsterite (Fo) = molar 100 × Mg/(Mg + Fe); Cr# = molar Cr/(Cr + Al). Error bars in panel C are 1σ. ΔFMQ is the deviation of logf_{O2} from the fayalite-magnetite-quartz buffer. (E,F) Plots of olivine δ^{18}O versus NiO and Fo. Gray shaded area represents δ^{18}O values of normal mantle olivine. Data sources for A–D and olivine fractionation model shown in E and F are given in the Supplemental Material (see footnote 1).

formation, because it contained phlogopite and had high δ^{18}O and f_{O2}. Mantle metasomatism by asthenosphere-derived, Fe-rich basaltic melts can lower the Mg/Fe ratios of the cratonic lower keel (Fig. 3B; Lee et al., 2011; Zheng et al., 2015). These Fe-rich basaltic melts responsible for refertilization of the SYC keel had high δ^{18}O and f_{O2} and were K- and CO_2-rich, and thus may have been derived by melting

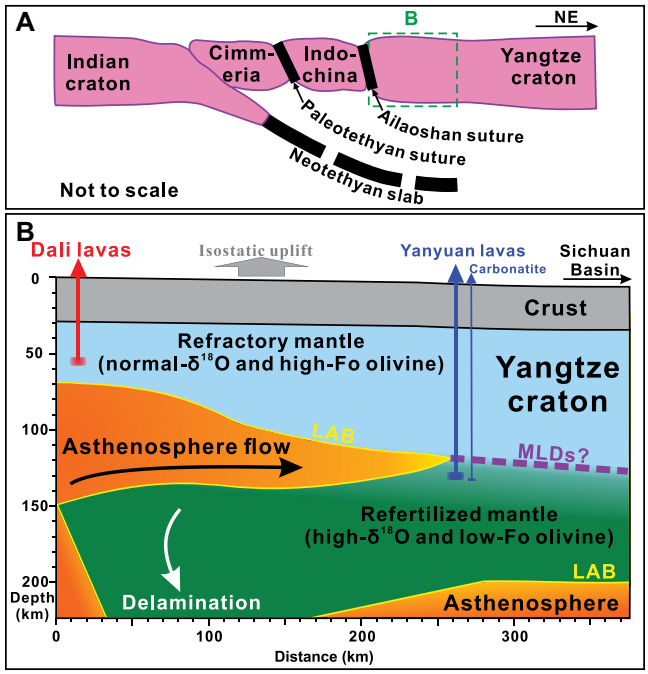

Figure 4. (A) Model of the southwestern Yangtze craton (China, SYC) mantle refertilization by northward subduction of multiple Tethyan oceans since the Paleozoic. (B) Schematic cross section of Eocene keel delamination in the SYC, based on Figure 1 and geobarometry results. Forsterite (Fo) = molar 100 × Mg/(Mg + Fe); MLDs—mid-lithospheric discontinuities; LAB—lithosphere-asthenosphere boundary.

of an asthenospheric wedge fluxed by liquids from subducted carbonate-bearing sediments. Given that oxygen is a major element, the changes in $\delta^{18}O$ require strong refertilization. Multiple subduction events beneath the SYC margin since the Paleozoic would have caused extensive refertilization of the SYC deep keel (Fig. 4A). Although small amounts of hydrous melts remaining from deep refertilization had oxidized and rehydrated the shallow harzburgite, they did not alter its refractory nature in terms of major elements.

Causes of Cratonic Keel Delamination

Seismic tomography suggests that the delaminated keel beneath the thinned SYC is not completely detached from the adjacent intact craton (Fig. 1C). Numerical modeling has shown that cratonic keel delamination can occur by peeling off a dense lower keel from the craton margin to the interior along weak mid-lithospheric discontinuities (MLDs; Liu et al., 2018). This explains the similar depths of the lithosphere-asthenosphere boundary (LAB) of thinned cratons and MLDs of adjacent intact cratons worldwide (Aulbach, 2018). During delamination of the SYC keel, hot asthenosphere flowed into the delaminating region and caused perturbation of the geotherm and melting of hydrated lithospheric mantle at various depths (Fig. 4B). The depth (131 ± 5 km) of the Yanyuan magma source is similar to that (~120 km; Fig. 1B) of the present-day LAB (i.e., the Eocene MLD), implying derivation from the upper part of the dense lower keel (Fig. 4B). The lower keel is more fertile and denser (i.e., low-Fo olivine) than the shallow mantle. The empirical relationship between the bulk density (ρ) of mantle peridotite and olivine Fo values (ρ = –0.0152 × Fo + 4.74; Lee, 2003) shows that a decrease in Fo values from 94.2 to 91.3 would increase the bulk density by ~0.044 g/cm^3. This density contrast was the major cause of the delamination of the dense lower keel and preservation of the buoyant shallow mantle (e.g., Liu et al., 2019). H_2O contents and f_{O2} values played a secondary role because both the shallow and deep mantle were hydrated and oxidized (Figs. 3C and 3D).

Refertilized peridotite in the SYC lower keel has a density (~3.35 g/cm^3) similar to that of fertile Phanerozoic lithosphere (3.36 ± 0.02 g/cm^3; Poudjom Djomani et al., 2001). It was buoyant when a high geothermal gradient existed in association with arc volcanism, but thermal contraction rendered it gravitationally unstable when magmatic lull and lithospheric thickening produced a low geotherm (Kay and Kay, 1993; Poudjom Djomani et al., 2001). Gradual eclogitization of Fe-rich infiltrated melts during cooling could have further increased the density (Liu et al., 2019). Thus, the continued India-Asia collision caused the thickening, cooling, and delamination of the SYC keel. The Eocene loss of this dense keel triggered surface uplift (Fig. 4B; Chung et al., 1998), as evident from the high topography of the thinned SYC (Fig. 1C). However, the compositionally unmodified refractory keel below the SYC interior remains buoyant.

A typical example of cratonic keel delamination during oceanic subduction occurred in the eastern North China craton in the Mesozoic (Fig. 1A; Wu et al., 2019). It became progressively denser in composition due to keel refertilization during subduction (Liu et al., 2019), but its keel delamination occurred mainly during the Cretaceous after Jurassic flat subduction of the paleo-Pacific slab (Wu et al., 2019). Both flat subduction and continental collision can cool and thermally densify the lithosphere through magmatic lull and compressional thickening, which finally triggers the delamination of a cratonic keel that has been compositionally densified during earlier subduction.

CONCLUSIONS

Our study reveals the nature of a delaminated cratonic keel, indicating that a combination of earlier refertilization and later cooling of the lithosphere, rather than hydration or oxidation, can cause its delamination due to compositional and thermal densification. Lithospheric refertilization results from prolonged subduction, and cooling may be related to magmatic lull and lithospheric thickening caused by continental collision or flat subduction. We therefore highlight the key roles of compositional and thermal densification in delamination during subduction and collision.

ACKNOWLEDGMENTS

We acknowledge editor Marc Norman, Claudio Chiarabba, and an anonymous reviewer for constructive suggestions. This study was supported by the Second Tibetan Plateau Scientific Expedition and Research (STEP) (grant 2019QZKK0702) and the National Natural Science Foundation of China (grants 42021002, 42002047, and 91855215). This is contribution IS-3155 of the Guangzhou Institute of Geochemistry, Chinese Academy of Sciences (GIGCAS).

REFERENCES CITED

Ammannati, E., Jacob, D.E., Avanzinelli, R., Foley, S.F., and Conticelli, S., 2016, Low Ni olivine in silica-undersaturated ultrapotassic igneous rocks as evidence for carbonate metasomatism in the mantle: Earth and Planetary Science Letters, v. 444, p. 64–74, https://doi.org/10.1016/j.epsl.2016.03.039.

An, M.J., and Shi, Y.L., 2006, Lithospheric thickness of the Chinese continent: Physics of the Earth and Planetary Interiors, v. 159, p. 257–266, https://doi.org/10.1016/j.pepi.2006.08.002.

Aulbach, S., 2018, Cratonic lithosphere discontinuities: Dynamics of small volume melting, metacratonization, and a possible role for brines, *in* Yuan, H.Y., and Romanowicz, B., eds., Lithospheric Discontinuities: American Geophysical Union Geophysical Monograph 239, p. 177–203, https://doi.org/10.1002/9781119249740.ch10.

Ballhaus, C., Berry, R.F., and Green, D.H., 1991, High pressure experimental calibration of the olivine-orthopyroxene-spinel oxygen geobarometer: Implications for the oxidation state of the upper mantle: Contributions to Mineralogy and Petrology, v. 107, p. 27–40, https://doi.org/10.1007/BF00311183.

Bindeman, I., 2008, Oxygen isotopes in mantle and crustal magmas as revealed by single crystal analysis: Reviews in Mineralogy and Geochemistry, v. 69, p. 445–478, https://doi.org/10.2138/rmg.2008.69.12.

Chung, S.L., Lo, C.H., Lee, T.Y., Zhang, Y.Q., Xie, Y.W., Li, X.H., Wang, K.L., and Wang, P.L., 1998, Diachronous uplift of the Tibetan plateau

starting 40 Myr ago: Nature, v. 394, p. 769–773, https://doi.org/10.1038/29511.

Cline, C.J., Faul, U.H., David, E.C., Berry, A.J., and Jackson, I., 2018, Redox-influenced seismic properties of upper-mantle olivine: Nature, v. 555, p. 355–358, https://doi.org/10.1038/nature25764.

Condamine, P., Médard, E., and Devidal, J.-L., 2016, Experimental melting of phlogopite-peridotite in the garnet stability field: Contributions to Mineralogy and Petrology, v. 171, 95, https://doi.org/10.1007/s00410-016-1306-0.

Fei, H.Z., Wiedenbeck, M., Yamazaki, D., and Katsura, T., 2013, Small effect of water on upper-mantle rheology based on silicon self-diffusion coefficients: Nature, v. 498, p. 213–215, https://doi.org/10.1038/nature12193.

Gavrilenko, M., Herzberg, C., Vidito, C., Carr, M.J., Tenner, T., and Ozerov, A., 2016, A calcium-in-olivine geohygrometer and its application to subduction zone magmatism: Journal of Petrology, v. 57, p. 1811–1832, https://doi.org/10.1093/petrology/egw062.

Hirth, G., and Kohlstedt, D.L., 1996, Water in the oceanic upper mantle: Implications for rheology, melt extraction and the evolution of the lithosphere: Earth and Planetary Science Letters, v. 144, p. 93–108, https://doi.org/10.1016/0012-821X(96)00154-9.

Hou, Z.Q., Liu, Y., Tian, S.H., Yang, Z.M., and Xie, Y.L., 2015, Formation of carbonatite-related giant rare-earth-element deposits by the recycling of marine sediments: Scientific Reports, v. 5, 10231, https://doi.org/10.1038/srep10231.

Huang, Z.C., Wang, L.S., Xu, M.J., Zhao, D.P., Mi, N., and Yu, D.Y., 2019, *P* and *S* wave tomography beneath the SE Tibetan Plateau: Evidence for lithospheric delamination: Journal of Geophysical Research: Solid Earth, v. 124, p. 10,292–10,308, https://doi.org/10.1029/2019JB017430.

Kamenetsky, V.S., Elburg, M., Arculus, R., and Thomas, R., 2006, Magmatic origin of low-Ca olivine in subduction-related magmas: Co-existence of contrasting magmas: Chemical Geology, v. 233, p. 346–357, https://doi.org/10.1016/j.chemgeo.2006.03.010.

Kay, R.W., and Kay, S.M., 1993, Delamination and delamination magmatism: Tectonophysics, v. 219, p. 177–189, https://doi.org/10.1016/0040-1951(93)90295-U.

Lee, C.-T.A., 2003, Compositional variation of density and seismic velocities in natural peridotites at STP conditions: Implications for seismic imaging of compositional heterogeneities in the upper mantle: Journal of Geophysical Research, v. 108, https://doi.org/10.1029/2003JB002413.

Lee, C.-T.A., Luffi, P., and Chin, E.J., 2011, Building and destroying continental mantle: Annual Review of Earth and Planetary Sciences, v. 39, p. 59–90, https://doi.org/10.1146/annurev-earth-040610-133505.

Lei, J.S., Zhao, D.P., Xu, X.W., Xu, Y.G., and Du, M.F., 2019, Is there a big mantle wedge under eastern Tibet?: Physics of the Earth and Planetary Interiors, v. 292, p. 100–113, https://doi.org/10.1016/j.pepi.2019.04.005.

Liu, L., Morgan, J.P., Xu, Y.G., and Menzies, M., 2018, Craton destruction 1: Cratonic keel delamination along a weak midlithospheric discontinuity layer: Journal of Geophysical Research: Solid Earth, v. 123, p. 10,040–10,068, https://doi.org/10.1029/2017JB015372.

Liu, L., Liu, L.J., Xu, Y.G., Xia, B., Ma, Q., and Menzies, M., 2019, Development of a dense cratonic keel prior to the destruction of the North China Craton: Constraints from sedimentary records and numerical simulation: Journal of Geophysical Research: Solid Earth, v. 124, p. 13,192–13,206, https://doi.org/10.1029/2019JB018595.

Lu, Y.J., McCuaig, T.C., Li, Z.X., Jourdan, F., Hart, C.J.R., Hou, Z.Q., and Tang, S.H., 2015, Paleogene post-collisional lamprophyres in western Yunnan, western Yangtze Craton: Mantle source and tectonic implications: Lithos, v. 233, p. 139–161, https://doi.org/10.1016/j.lithos.2015.02.003.

Mattey, D., Lowry, D., and Macpherson, C., 1994, Oxygen-isotope composition of mantle peridotite: Earth and Planetary Science Letters, v. 128, p. 231–241, https://doi.org/10.1016/0012-821X(94)90147-3.

Poudjom Djomani, Y.H., O'Reilly, S.Y., Griffin, W.L., and Morgan, P., 2001, The density structure of subcontinental lithosphere through time: Earth and Planetary Science Letters, v. 184, p. 605–621, https://doi.org/10.1016/S0012-821X(00)00362-9.

Prelević, D., and Foley, S.F., 2007, Accretion of arc-oceanic lithospheric mantle in the Mediterranean: Evidence from extremely high-Mg olivines and Cr-rich spinel inclusions in lamproites: Earth and Planetary Science Letters, v. 256, p. 120–135, https://doi.org/10.1016/j.epsl.2007.01.018.

Straub, S.M., LaGatta, A.B., Martin-Del Pozzo, A.L., and Langmuir, C.H., 2008, Evidence from high-Ni olivines for a hybridized peridotite/pyroxenite source for orogenic andesites from the central Mexican Volcanic Belt: Geochemistry Geophysics Geosystems, v. 9, Q03007, https://doi.org/10.1029/2007GC001583.

Wang, Y.J., Qian, X., Cawood, P.A., Liu, H.C., Feng, Q.L., Zhao, G.C., Zhang, Y.H., He, H.Y., and Zhang, P.Z., 2018, Closure of the East Paleotethyan Ocean and amalgamation of the Eastern Cimmerian and Southeast Asia continental fragments: Earth-Science Reviews, v. 186, p. 195–230, https://doi.org/10.1016/j.earscirev.2017.09.013, corrigendum available at https://doi.org/10.1016/j.earscirev.2021.103636.

Wu, F.Y., Yang, J.H., Xu, Y.G., Wilde, S.A., and Walker, R.J., 2019, Destruction of the North China Craton in the Mesozoic: Annual Review of Earth and Planetary Sciences, v. 47, p. 173–195, https://doi.org/10.1146/annurev-earth-053018-060342.

Yang, H.Y., Peng, H.C., and Hu, J.F., 2017, The lithospheric structure beneath southeast Tibet revealed by P and S receiver functions: Journal of Asian Earth Sciences, v. 138, p. 62–71, https://doi.org/10.1016/j.jseaes.2017.02.001.

Zheng, J.P., Lee, C.-T.A., Lu, J.G., Zhao, J.H., Wu, Y.B., Xia, B., Li, X.Y., Zhang, J.F., and Liu, Y.S., 2015, Refertilization-driven destabilization of subcontinental mantle and the importance of initial lithospheric thickness for the fate of continents: Earth and Planetary Science Letters, v. 409, p. 225–231, https://doi.org/10.1016/j.epsl.2014.10.042.

Printed in USA